

# Towards automatic cell identification in DIC microscopy

D. Young<sup>1</sup>, C.A. Glasbey<sup>2†</sup>, A.J. Gray<sup>1</sup> and N.J. Martin<sup>3</sup>

<sup>1</sup> Department of Statistics and Modelling Science, University of Strathclyde  
Livingstone Tower, 26 Richmond Street, Glasgow G1 1XH, Scotland

<sup>2</sup> Biomathematics and Statistics Scotland  
JCMB, King's Buildings, Edinburgh EH9 3JZ, Scotland

<sup>3</sup> Biochemical Sciences Department, Scottish Agricultural College  
Auchincruive, Ayr KA6 5HW, Scotland

† Corresponding author

## Abstract

A general method is proposed for constructing templates of cells in differential interference contrast (DIC) microscopy. This takes account of the optics which generate DIC images, and is applicable to both transparent and semi-transparent cells of simple and complex shapes. Then, a template matching methodology is presented, which uses Fast Fourier Transforms to fit templates of a range of sizes and orientations to images. For illustration, this is used to automatically identify and measure individual *Candida* yeast cells in clusters.

## 1 Introduction

Quantitative aspects of microscopy are increasingly important in many fields. In microbial ecology it is widely recognised that simply counting cell numbers gives a misleading analysis of microbial ecosystems: biomass estimation is essential as well. For example, Jenkinson, Powelson and Wedderburn (1976) showed that the product of cell number and cell biomass was roughly constant over a wide range of cell sizes: scarcer, large microbial cells made a total contribution to the microbial biomass in soil similar to that of the more numerous small cells. Visual procedures for estimating cell numbers and cell size have been used in the past but the procedures are so time consuming as to severely limit their application, presenting a clear target for automation.

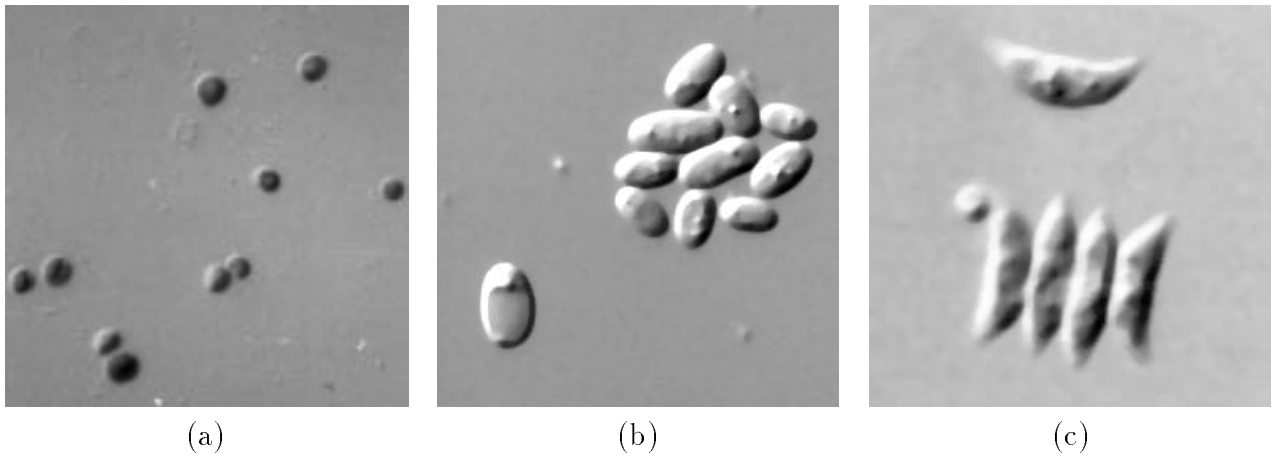


Figure 1: DIC microscope images: **(a)** *Chlorella* algal cells, **(b)** *Candida* yeast cells, **(c)** *Scenedesmus* algal cells.

Automated microscopy requires the computer to identify, count and measure cells or cell features. Cytological investigations are increasingly using these tools to quantify and analyse features as diverse as the nuclei in Papanicolaou stained cervical smears (Walker, Jackway and Lowell, 1995), immunochemically labelled neurons in cerebral cortex sections (Hibbard et al., 1996) and fluorescent stained fungal hyphae in decomposing leaves (Daniel, Schonholzer and Zeyer, 1995). In all these cases the staining generates sufficient contrast between the features of interest and the rest of the image to allow the investigator to address the problems of interpreting the image features with the attendant difficulties caused by overlapping cells, different cell types or out of focus material.

Living unstained cells require the application of optical techniques to generate contrast with their surroundings for satisfactory thresholding. The two most widely used methods for examining living cells are differential interference contrast (DIC) and phase contrast. DIC is better suited for image analysis since cell edges are not clearly defined using phase contrast because of the halo of defocused light around areas of high optical contrast. Although clearly defined to the human eye, DIC-visualised cells pose a significant challenge to automated image interpretation because of the pseudo bas-relief image. One side of cells is lighter than the background and the other side is darker, with a neutral point in between where a cell's edge intensity equals the background intensity (see Fig 1). Image segmentation algorithms using either thresholding or edge tracking methods typically fail with such images.

The cause of this problem is due to the appearance of the DIC image, which is due to the way the DIC image is formed. A plane polarised beam of light is split into two mutually coherent, orthogonally-polarised components by the substage compensator Wollaston prism (see Slayter and Slayter, 1992, pp 154-158). The two components are phase shifted relative to each other (bias retardation) and laterally displaced (shear) by a few tenths of a micrometre. Each of the split beams passes through a close but separate part of the specimen, where its phase is shifted by a further amount, depending on the optical path length (i.e. product of refractive index and geometric path length) through the specimen. The beams are recombined by a second, sliding Wollaston prism, near the back focal plane of the objective, which is adjustable by translation of

the prism and controls the appearance of the final image. A final polarising filter, the analyser, converts the phase differences into amplitude differences.

Usually the bias retardation is set so that an optically-uniform part of the specimen is grey, increasing optical gradients (strictly, gradients in the specimen's phase function) in the direction of shear appear brighter, and decreasing gradients appear darker. The intensity will depend on the gradient and its orientation. Gradients in the direction of shear will show the greatest intensity change, while gradients oriented at  $90^\circ$  to this direction will produce no phase shift between the beams and so show no change in intensity. This dependence of image intensity on the gradient orientation is responsible for the two neutral points in a cell outline and the false illusion that the DIC image is three dimensional. As shown below, however, information on the third dimension is present and integration of the image intensity can give an image of the optical thickness of the specimen.

Template matching, in which the best agreement is sought between a known prototype and an image (see, for example, Gonzalez and Woods, 1992, pp 583-586), offers a methodology for automating the identification and measuring of cells in microscope images. Correspondences are found between a template sub-image and the full image, based on a goodness-of-fit statistic evaluated at all possible positions. It is a computationally-expensive procedure, especially when multiple templates are involved. Ordered matching, multi-stage matching and hierarchical matching have been proposed to reduce the number of computations. Margalit and Rosenfeld (1990a) used probabilistic information, such as grey-level histograms from the image and template, to order the computations of a matching criterion. Goshtasby *et al.* (1984) proposed a two-stage approach, using a sub-template initially to determine good candidate locations for a match, then applying the whole template in the second stage only to locations identified by the sub-template. Goshtasby (1985) used normalised invariant moments as a first-stage similarity measure, whereas Margalit and Rosenfeld (1990b) used a template feature which occurred only rarely. Anisimov and Gorsky (1993) considered matching at multiple resolutions. Parallel algorithms have been considered by Prasanna-Kumar and Krishnan (1989) and Sid-Ahmed (1990). For certain classes of matching criteria, substantial reductions in time can be achieved by using Fast Fourier Transforms (see, for example, Glasbey and Horgan, 1995, pp 60-69). These strategies are all effective for reducing computer time, but in all cases at the cost of increased computer programming complexity. We have only found it necessary to use Fast Fourier Transforms in this paper in order to reduce computer time to an acceptable level. However, ordered matching, multi-stage matching and hierarchical matching strategies could all be deployed to reduce times further.

In section 2, a general method is proposed for constructing templates of DIC images of cells. Then, in section 3, a template matching methodology is presented and illustrated. This is a first stage towards dealing with the more complex images presented by specimens prepared from mixed microbial populations with different cell morphologies, overlapping and out of focus cells.

## 2 Template construction

To apply template matching, we need a model or sub-image of a single cell, typical of the cells to be identified in the image. We shall consider three variants of an approach to template construction. In section 2.1, cells with simple geometrical shapes, such as the *Chlorella* algal cells in Fig 1a, are modelled. Then, in section 2.2, transparent cells such as the *Candida* yeast cells in Fig 1b are considered. Finally, in section 2.3, a method for constructing templates is proposed for semi-transparent cells of general shape, by making use of auxiliary brightfield microscope images.

### 2.1 Geometrically shaped cells

For cells which have simple geometrical shapes, we can use the theory of DIC microscopy to construct templates. For example, a spherical cell with radius  $r$ , centred at  $(i_0, j_0)$ , has thickness at location  $(i, j)$ , indexed by row index  $i$  and column index  $j$ , specified by

$$t(i, j) = \begin{cases} 2\sqrt{r^2 - (i - i_0)^2 - (j - j_0)^2} & \text{if } (i - i_0)^2 - (j - j_0)^2 \leq r^2 \\ 0 & \text{otherwise.} \end{cases}$$

If, for simplicity, we assume that the cell has constant optical density, then the light passing through it will be attenuated in accord with Beer's Law (Slayter and Slayter, 1992, p 97), giving

$$B(i, j) = ae^{-bt(i, j)}.$$

Here,  $B(i, j)$  is the image intensity at location  $(i, j)$  that would be observed in a brightfield microscope image, and  $a$  and  $b$  are non-negative constants. If we also assume that the cell has constant refractive index, so that phase change is proportional to thickness, and for simplicity standardise on beam shear of  $(+\Delta, +\Delta)$  and a bias retardation of  $90^\circ$  (as in Fig 1), then for diffraction-free optics the DIC image is given by

$$F(i, j) = \frac{1}{2}B(i, j) + \frac{1}{2}B(i + \Delta, j + \Delta) + \sqrt{B(i, j)B(i + \Delta, j + \Delta)} \sin [c \{t(i, j) - t(i + \Delta, j + \Delta)\}]$$

where  $c$  is a constant (Holmes and Levy, 1987; Cogswell and Sheppard, 1992). We can simplify this expression using linearising approximations. For example, the first term in a Taylor's series expansion gives

$$B(i + \Delta, j + \Delta) \approx B(i, j) + \sqrt{2}\Delta \frac{\partial B(i, j)}{\partial v} = B(i, j) \left( 1 - \sqrt{2}\Delta b \frac{\partial t(i, j)}{\partial v} \right),$$

where  $v$  ( $= i + j$ ) is the direction of shear and  $\partial/\partial v$  is a directional derivative. After some algebra, we obtain

$$F(i, j) \approx B(i, j) \times D(i, j), \quad \text{where} \quad D(i, j) = 1 + c' \frac{\partial t(i, j)}{\partial v}$$

and  $c'$  is a constant which depends on  $a$ ,  $b$  and  $c$ . In particular, if the specimen is completely transparent, we obtain the pure DIC image,  $D(i, j)$ , with image intensity proportional to the directional rate of change of optical thickness, as reported by Holmes and Levy (1987).

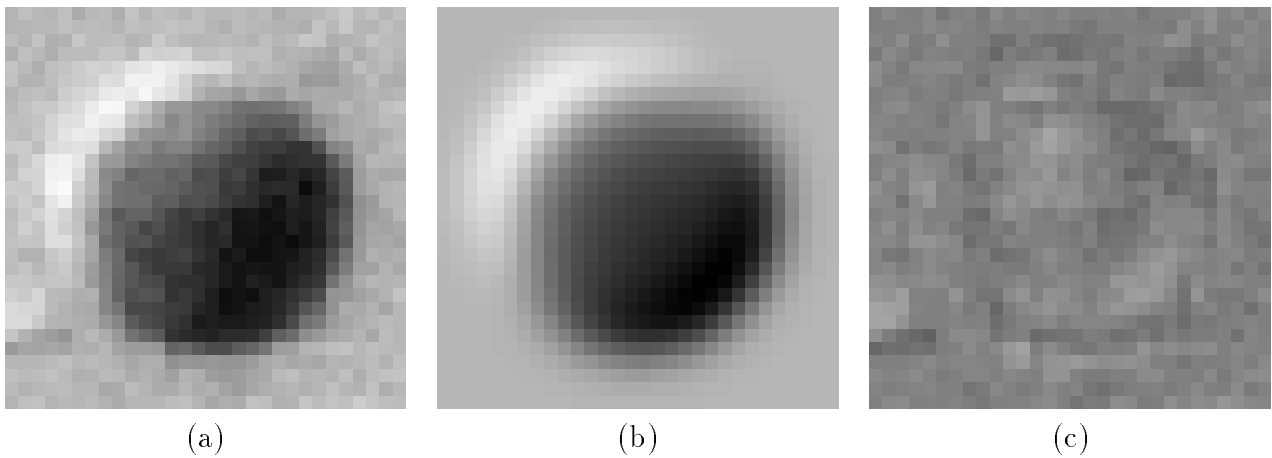


Figure 2: A single *Chlorella* algal cell: **(a)** image extracted from Fig 1a, **(b)** fitted model, **(c)** residuals (rescaled so that zero displayed as mid-grey).

We further assume that the response of the digitising camera is linear with respect to intensity, after a baseline shift. These parameters, together with  $i_0$ ,  $j_0$ ,  $r$ ,  $a$ ,  $b$  and  $c$  were chosen using a numerical optimisation algorithm, to give the best match with Fig 2a, which shows the right-most *Chlorella* algal cell in Fig 1a, by minimising the sum of squares of differences between the data and the fitted model (for further details, see Young, 1997). The fit was improved substantially if  $F$  was convolved with a Gaussian point spread function with standard deviation  $\sigma$ , which was also estimated. If blur were solely due to the microscope optics, then more appropriate point spread functions could have been used (Hopkins, 1955; Sheppard and Gu, 1991), and they could have been applied in the complex domain, to take account of phase as well as amplitude effects (Preza, Snyder and Conchello, 1996). However, we have taken a pragmatic view that the blur in Fig 2a has multiple sources, such as the effects of the digitising camera and the three-dimensional nature of the specimen, and that for a small amount of blur the exact form of the point spread function is not critical. The estimated image, incorporating Gaussian blur, is shown in Fig 2b. Fig 2c shows the difference between the data and the fit, from which it can be seen that the model fits very well: the model accounts for 96.4% of the variation in pixel values in Fig 2a. Fig 2b could, after rescaling to take account of different cell sizes, be used as a template to identify the remaining algal cells in Fig 1a. Alternatively, and more simply, if sampling errors are small, then Fig 2a could be used directly as a template.

## 2.2 Transparent cells

If cells are not spherical and lie at varying orientations, then it is not possible to use a single cell as a template because, if the template is rotated, its direction of DIC beam displacement also rotates, whereas to match with the image it needs to remain fixed. Such is the case with the *Candida* yeast cells in Fig 1b; after rotation, the light side of the cell would no longer be on the top left side of the cell. The yeast cells are approximately ellipsoidal in shape and could, therefore, be modelled at each of a range of orientations using similar methods to section 2.1, perhaps using super-ellipses (Pilu *et al.*, 1996). However, because they are transparent, we

can avoid having to assume a particular geometric shape by using a more general approach to template construction.

We shall use the isolated yeast cell in the bottom left corner of Fig 1b as the basis for a template. If an object is completely transparent, as this cell is, then the brightfield component of the image can be ignored: DIC microscopy produces a pure DIC image,  $D(i, j)$ , with image intensity proportional to the directional rate of change of optical thickness. This differentiation can be reversed, by integrating image intensities in direction  $v$ , to produce an image of optical thickness (Glasbey and Martin, 1996). If such an image is rotated, then differenced in direction  $v$ , we obtain a valid DIC template at another orientation. We have found this simple approach effective. For more-sophisticated phase estimation methods, see van Munster, van Vliet and Aten (1997), Preza, Snyder and Conchello (1997) and Preza et al. (1997).

The sub-image of the isolated yeast cell was mean corrected, and integrated along the diagonals from top left to bottom right using

$$F'(i, j) = \sum_{k=0}^{\min(i,j)-1} (F(i-k, j-k) - \bar{F}),$$

where  $\bar{F}$  denotes the mean pixel value in the sub-image. Then the diagonals are rescaled (to reduce streaking) using, for an  $n \times n$  image,

$$F''(i, j) = \begin{cases} F'(i, j) - \frac{i}{n+i-j} F'(i-j+n, n) & \text{if } i \leq j, \\ F'(i, j) - \frac{j}{n-i+j} F'(n, j-i+n) & \text{otherwise,} \end{cases}$$

which sets the cumulative sums to zero at the borders of the image (Glasbey and Martin, 1996). After application of a  $7 \times 7$  median filter to smooth the output, the resulting image of optical thickness is shown in Fig 3a. (Note, if it were possible to obtain such a good result by applying the same algorithm to Fig 1b, then we could identify cells simply by thresholding the transformed image. However, this is not possible because the method only works for small sub-images, otherwise the cumulative effects of noise swamp the image.) The final step in the template construction is to rotate Fig 3a to a new orientation and differentiate. For example, Fig 3b shows the template for a cell after a rotation of  $45^\circ$ . This template can be rescaled using bilinear interpolation (see, for example, Glasbey and Horgan, 1995, p 42), to produce templates with a range of orientations and sizes for use with the matching algorithm.

## 2.3 Other cells

If cells are not geometric in shape and are only semi-transparent, such as the pigmented *Scenedesmus* algal cells in Fig 1c, then neither of the above approaches will work. However, if we have a brightfield image of the same cells, co-registered with the DIC image (Glasbey and Martin, 1996), as is the case with Fig 4a, then we can proceed. If pixel values in the DIC image are element-by-element divided by those in the brightfield image:

$$D(i, j) = \frac{F(i, j)}{B(i, j)},$$

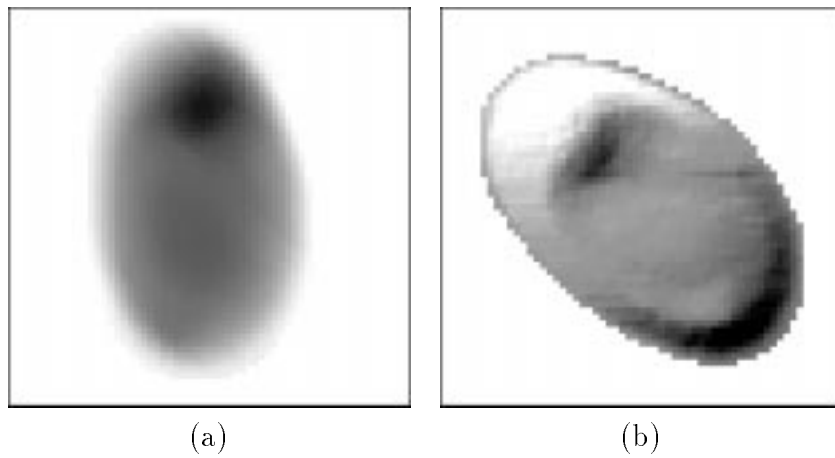


Figure 3: *Candida* yeast cell: (a) estimated optical thickness, (b) example of template for cell at orientation of  $45^\circ$ .

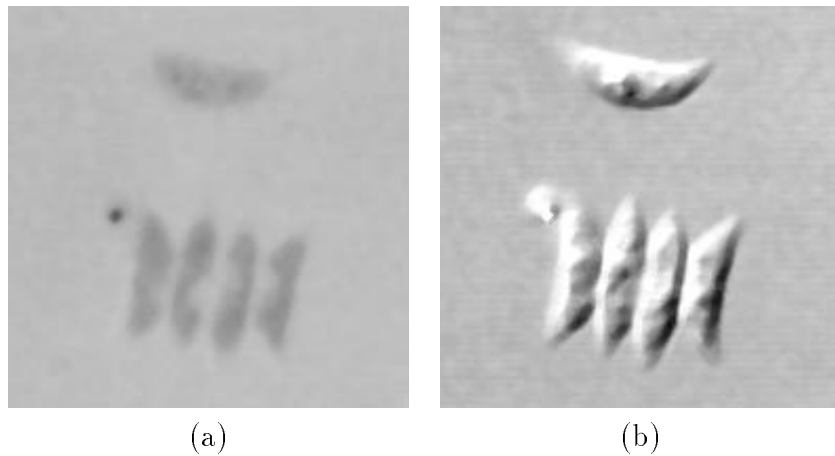


Figure 4: *Scenedesmus* algal cells: (a) brightfield image, (b) DIC image after correction for light absorption shown in brightfield image.

then an image purely of the rate of change of the optical thickness of the specimen is produced. This is an approximation, which seems to work better than subtracting the brightfield image, used by Glasbey and Martin (1996). A more sophisticated approach has been proposed by Cogswell et al. (1997), using DIC images at four different bias retardations. Fig 4b shows the result of dividing Fig 1c by Fig 4a: it is as though the *Scenedesmus* algal cells were transparent. Fig 4b can now be analysed using the methods in section 2.2.

### 3 Template matching

Many template matching criteria have been proposed (see, for example, Young, 1997). One of the simplest and easiest to understand and use is the mean square difference:

$$G(i, j) = \frac{1}{N_S} \sum_{(k,l) \in S} \{F(i+k, j+l) - T(k, l)\}^2,$$

where  $S$  is the set of lattice points for which the template is defined,  $N_S$  denotes the number of such points, and  $T(k, l)$  is the array of values in the template. A good match at location  $(i, j)$  in the image is indicated by a small value of  $G(i, j)$ . This matching criterion is one for which Fast Fourier Transforms (FFTs) can be used to substantially reduce the number of computations. We can re-express  $G$  as

$$G(i, j) = \frac{1}{N_S} \sum_{(k,l) \in S} F^2(i+k, j+l) - \frac{2}{N_S} \sum_{(k,l) \in S} F(i+k, j+l)T(k, l) + \frac{1}{N_S} \sum_{(k,l) \in S} T^2(k, l).$$

The first sum is a convolution between  $F^2$  and the indicator function for set  $S$ , the second sum is a convolution or correlation between  $F$  and  $T$ , and the third sum is a constant, the sum-of-squares of the elements in  $T$ . The two convolutions can be computed for all values of  $(i, j)$  simultaneously, by Fourier-transforming their parts, performing an element-by-element multiplication, then back-transforming (see, for example, Glasbey and Horgan, 1995, p 68). Computations were sufficiently fast that we did not need to resort to the methods discussed in section 1, of ordered, multi-stage or hierarchical matching. However, note that one disadvantage of the Fourier approach is that templates which overlap the boundary of an image are wrapped-round and the missing parts appear at the other side of the image. This affects sampling properties for cells which intersect an image boundary, although it is not critical for the images in Figure 1.

In general, a separate template has to be defined for each of a range of sizes and orientations of cells. Let  $G_{LWO}$  denote the mean square differences obtained for a template with length  $L$ , width  $W$  and orientation  $O$ . Output from multiple templates is specified by

$$H(i, j) = \min_{(L,W,O)} G_{LWO}(i, j).$$

We restrict attention to local minima of  $H$ , namely locations  $(i, j)$  such that

$$H(i, j) \leq H(k, l) \quad \text{for } k = i, i \pm 1; \quad l = j, j \pm 1.$$

The smallest of the local minima of  $H$  is found, and the corresponding values of  $i, j, L, W$  and  $O$  which identify the best fitting template. Once this cell has been identified, we no longer allow another template to be identified which overlaps this one. Therefore we eliminate from subsequent search all positions  $(i, j)$  for which the best template overlaps this one. We then repeat the procedure, minimising  $H$  and again eliminating all overlapping templates. We do this repeatedly until some stopping criterion is reached.

We will illustrate the methodology by using the *Candida* yeast template constructed in section 2.2 to interpret Fig 1b. Twenty five sizes of template were used, by varying the overall size

	1	2	3	4	5	6	7	8	9	10	11	12	13	14	15
$H$	848	1124	1247	1360	1452	1477	1661	1661	1888	1982	2007	3011	3083	3264	3265

Table 1: Fifteen smallest values of  $H$  obtained when fitting templates to *Candida* yeast cells in Fig 1b.

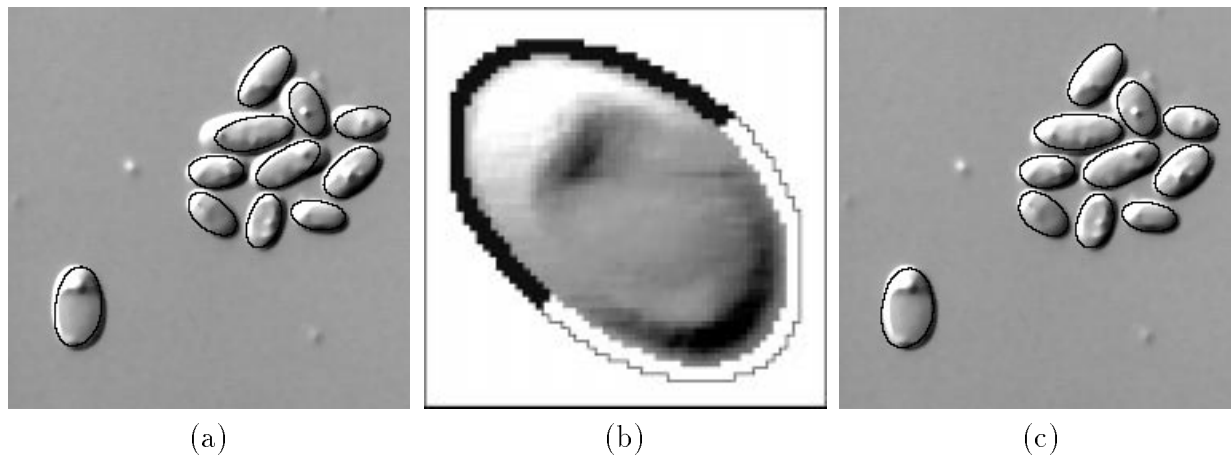


Figure 5: *Candida* yeast cells with identified cell boundaries superimposed: **(a)** first results, **(b)** example of modified template (see text), **(c)** results using modified template.

from 70% to 110% of that in Fig 3b, in 10% steps, and varying the length to width ratio from 70% to 110% of that in Fig 3b, also in 10% steps. For each template, 18 orientations were used, in 10° increments. The computations for fitting 450 templates to a  $250 \times 250$  image took 290 seconds of CPU time on a Sun Ultra 170. In determining whether templates overlapped, the cell boundary was shrunk by 2 pixels from the template boundary visible in Fig 3b, in case touching cells produced slightly overlapping templates. Table 1 shows the fifteen smallest values of  $H$ , from which we see that there is a large increase in values between the eleventh and twelfth possible cell: the increase exceeds both 1000 and 50%. We therefore have a strong indication that there are eleven cells in Fig 1b, and Fig 5a shows the result.

We can see that the results in Fig 5a are reasonable, except that cell sizes have been underestimated. This is because the templates fit both interiors of cells and whole cells almost equally well. One way of overcoming this, considered by Young (1997), is to fit templates in descending order of size. Here we followed a different approach, by including a border of 2 pixels, set to background values, round each cell template. However, this had the undesirable effect of the matching failing to identify some touching cells. Therefore, as a second modification, border pixels were set to the values they would encounter if there were touching cells, namely, black above and to the left of the template and white below and to the right. One such template is shown in Fig 5b. When these templates were used, the final result is as shown in Fig 5c. The boundaries of all cells have been located accurately. To quantify this, the lengths and breadths of the eleven cells were also measured by manually from Fig 1b. For calibration, all measurements are expressed in proportion to the template cell. Fig 6 shows the two sets of measurements plotted against each other. If we assume that the manual results are totally

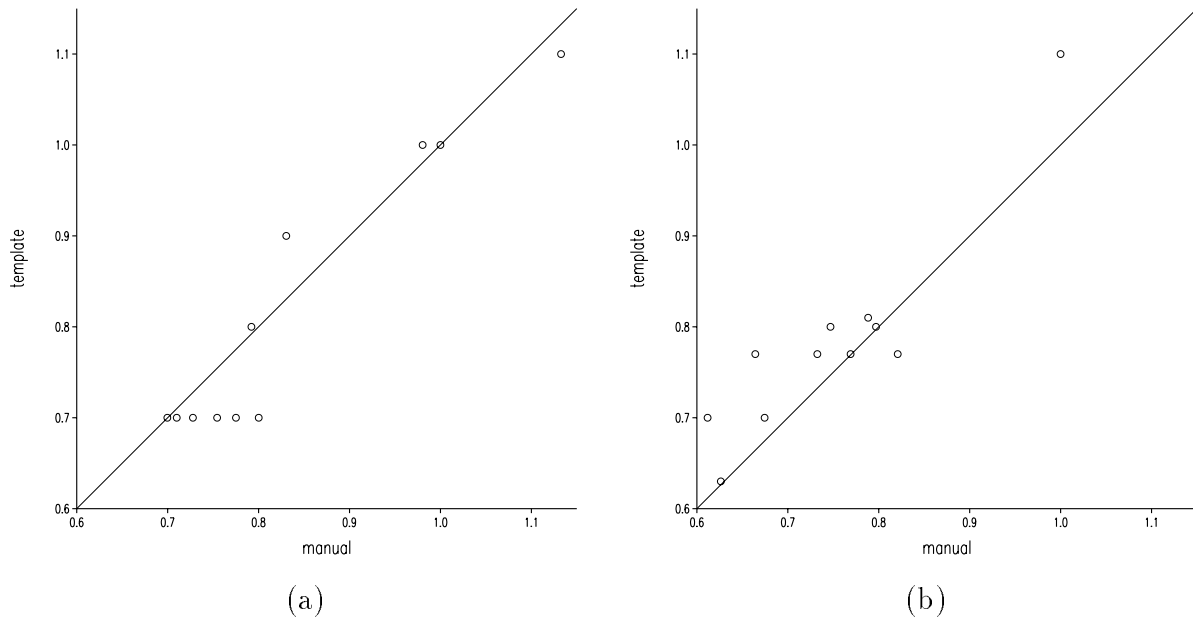


Figure 6: *Candida* yeast cell dimensions estimated by template fitting plotted against manual results, together with a 1:1 line: **(a)** length, **(b)** breadth. (Measurements are expressed in proportion to the template cell).

accurate, then the root-mean-square error in the template results is 0.05 for length and 0.06 for breadth. This could be reduced further by using a finer mesh of template sizes and empirically calibrating the template results against the manual ones.

## 4 Discussion

Template matching has demonstrated its potential for the automatic identification and measurement of microbial cells in DIC images, and therefore to offer a route towards automated microscopical counts of microbial cells in natural ecosystems. A general method has been presented for constructing templates to represent microbial cells in DIC microscope images, together with a procedure for identifying, counting, and sizing the cells in such images. The methods can be applied directly to images of transparent cells of different shapes captured by DIC microscopy. Light absorption by cells with complex-shaped light-absorbing structures such as algal chloroplasts can be taken account of using auxiliary brightfield microscope images, thereby extending the method to deal with semi-transparent cells.

The work in this paper is but a first step in the automatic measurement of microbial cells. The DIC images in Fig 1 are relatively simple, consisting as they do of in-focus monolayers of single populations on featureless backgrounds. Further work is needed to extend the method to deal with images of mixed populations such as the example shown in Glasbey and Martin (1996). In these preparations there may be cells with optically well defined internal features such as

spores or vacuoles, out of focus cells and overlapping cells. Internal cell structures may be discounted by the automatic rejection of features enclosed in other features. With out of focus cells, bright features will tend to be enlarged and dark features contracted by the redistribution of light in the extrafocal images. Setting suitable edge criteria will lead to the rejection of out of focus cells but at the expense of lost data from the rejected cells. The methodology also has to ensure that overlapping cells can be satisfactorily measured and further investigations are in progress to develop this aspect of template matching.

## Acknowledgements

DY was supported by an Earmarked Studentship from the Engineering and Physical Sciences Research Council. CAG and NJM were supported by funds from the Scottish Office Agriculture, Environment and Fisheries Department.

## References

Anisimov, V.A. and Gorsky, N.D. (1993). Fast hierarchical matching of an arbitrarily oriented template. *Pattern Recognition Letters*, **14**, 95-101.

Cogswell, C.J. and Sheppard, C.J.R. (1992). Confocal differential interference contrast (DIC) microscopy: including a theoretical analysis of conventional and confocal DIC imaging. *Journal of Microscopy*, **165**, 81-101.

Cogswell, C.J., Smith, N.I., Larkin, K.G. and Hariharan, P. (1997). Quantitative DIC microscopy using a geometric phase shifter. *Proceedings of the SPIE Symposium in Three-Dimensional Microscopy: Image Aquisition and Processing IV*, **2984**, 72-81.

Daniel, O., Schonholzer, F. and Zeyer, J. (1995). Quantification of fungal hyphae in leaves of deciduous trees by automated image-analysis. *Applied Environmental Microbiology*, **61**, 3910-3918.

Glasbey, C.A. and Horgan, G.W. (1995). *Image Analysis for the Biological Sciences*. Wiley, Chichester.

Glasbey, C.A. and Martin, N.J. (1996). Multimodality microscopy by digital image processing. *Journal of Microscopy*, **181**, 225-237.

Gonzalez, R.C. and Woods, R.E. (1992). *Digital Image Processing*. Addison-Wesley, Massachusetts.

Goshtasby, A. (1985). Template matching in rotated images. *IEEE Transactions on Pattern Analysis and Machine Intelligence*, **7**, 338-344.

- Goshtasby, A., Gage, S.H. and Bartholic, J.F. (1984). A two-stage cross correlation approach to template matching. *IEEE Transactions on Pattern Analysis and Machine Intelligence*, **6**, 374-378.
- Hibbard, L.S., McCasland, J.S., Brunstom, J.E. and Pearlman, A.L. (1996). Automated recognition and mapping of immunolabelled neurones. *Journal of Microscopy*, **183**, 241-256.
- Holmes, T.J. and Levy, W.J. (1987). Signal-processing characteristics of differential interference contrast microscopy. *Applied Optics*, **26**, 3929-3939.
- Hopkins, H.H. (1955). The frequency response of a defocused optical system. *Proceedings of the Royal Society (London) A*, **231**, 91-103.
- Jenkinson, S.D., Powlson, D.S. and Wedderburn, R.W.M. (1976). The effects of biocidal treatments on metabolism in soil. III. *Soil Biology and Biochemistry*, **8**, 189-202.
- Margalit, A. and Rosenfeld, A. (1990a). Using probabilistic domain knowledge to reduce the expected computational cost of template matching. *Computer Vision, Graphics and Image Processing*, **51**, 219-234.
- Margalit, A. and Rosenfeld, A. (1990b). Using feature probabilities to reduce the expected computational cost of template matching. *Computer Vision, Graphics and Image Processing*, **52**, 110-123.
- Pilu, M., Fitzgibbon, A.W. and Fisher, R.B. (1996). Training PDMs on models: the case of deformable superellipses. *Proceedings of the 7th British Machine Vision Conference*, Edinburgh, Scotland, 373-382.
- Prasanna-Kumar, V.K. and Krishnan, V. (1989). Efficient parallel algorithms for image template matching on hypercube SIMD machines. *IEEE Transactions on Pattern Analysis and Machine Intelligence*, **11**, 665-669.
- Preza, C., Snyder, D.L. and Conchello, J-A. (1996). Imaging models for three-dimensional transmitted-light DIC microscopy, *Proceedings of the SPIE Symposium on Electronic Imaging, Science and Technology*, **2655**, 245-257.
- Preza, C., Snyder, D.L. and Conchello, J-A. (1997). Image reconstruction for three-dimensional transmitted-light DIC microscopy, *Proceedings of the SPIE Symposium in Three-Dimensional Microscopy: Image Aquisition and Processing IV*, **2984**, 220-231.
- Preza, C., Snyder, D.L., Rosenberger, F.U., Markham, J. and Conchello, J-A. (1997). Phase estimation from transmitted-light DIC images using rotational diversity, *Proceedings of the SPIE Symposium on Image Reconstruction and Restoration II*, **3170**, 97-107.
- Sid-Ahmed, M.A. (1990). Serial architectures for the implementation of 2-D digital filters and for template matching in digital images. *IEEE Transactions on Acoustics, Speech and Signal Processing*, **38**, 853-857.
- Slyter, E.M. and Slyter, H.S. (1992). *Light and Electron Microscopy*. Cambridge University

Press.

Sheppard, C.J.R. and Gu. M. (1991). Approximation to the three-dimensional optical transfer function. *Journal of the Optical Society of America A*, **8**, 692-694.

van Munster, E.B., van Vliet, L.J. and Aten, J.A. (1997). Reconstruction of optical pathlength distributions from images obtained by a wide-field differential contrast microscope. *Journal of Microscopy*, **188**, 149-157.

Walker, R.F., Jackway, P. and Lovell, B. (1995). Cervical cell classification via co-occurrence and Markov random field features. In *DICTA 95 – Third Conference on Digital Image Computing: Techniques and Applications: Australian Pattern Recognition Society*, Brisbane, Australia. pp.294–299.

Young, D. (1997). *Cell Identification in Microscope Images*. Doctoral Thesis, University of Strathclyde.